Available online at www.sciencedirect.com
SCIENCE DIRECT®
Journal of Chromatography A, 1062 (2005) 275–283
JOURNAL OF CHROMATOGRAPHY A
www.elsevier.com/locate/chroma

Direct observation of frits and dynamic air bubble formation in capillary electrochromatography using confocal fluorescence microscopy

Gufeng Wang, Mark Lowry, Zhenming Zhong, Lei Geng*

Department of Chemistry, The Optical Science and Technology Center and The Center for Biocatalysis and Bioprocessing, University of Iowa, Iowa City, IA 52242, USA

Received 12 May 2004; received in revised form 12 November 2004; accepted 12 November 2004
Available online 8 December 2004

Abstract

Confocal fluorescence microscopy has been used to study the capillary electrochromatography (CEC) frits and dynamic air bubble formation under real chromatographic conditions. Confocal fluorescence microscopy provides a nondestructive way to view the three-dimensional structure of the frits with high spatial resolution. Frits prepared with four different procedures were studied: (1) sintering bare silica beads with sodium silicate; (2) sintering bare silica beads wetted with water; (3) sintering C18 beads wetted with water; and (4) sintering C18 beads wetted with water and then surfaced-recovered with C18. Frits prepared with sintering silicate-wetted beads have a high degree of heterogeneity, while the other three types of frits have similar, more homogeneous packing structures. Confocal fluorescence microscopy also provides sufficient temporal resolution for in situ observation of the dynamic processes in air bubble formation. In this study, air bubble formation is imaged during the reorganization process of the packing bed and is shown to occur close to the border between the packing bed and the outlet frit. Confocal fluorescence microscopy opens a new avenue in studying dynamic processes in situ in CEC separations.

Keywords: Confocal fluorescence microscopy; Capillary electrochromatography; Frits; Bubble formation

1. Introduction

In conventional packed-column capillary electrochromatography (CEC), the preparation of the frits is central to the making of a column. The quality of the frits affects separation efficiency and sensitivity of the column. Many problems in separations are associated with the frits, for example, tailing, column fragility and air bubble formation [1,2]. The initial frit preparation methods in pioneering work of CEC are either using sol–gel reactions [3,4] or by sintering silicate-wetted chromatographic beads [5]. Frits prepared with these two methods have the best mechanical stability and sufficient permeability. Subsequently, methods were pursued for improved reproducibility in the electric current and permeability of the columns. Behnke et al. reported that frit made from sintering beads soaked with pure water gives the column a stable condition of electroosmotic flow and a stable baseline, well suited for CEC [6]. Rebscher and Pyell's study confirmed that frits prepared with this method exhibit high permeability and the absence of bubble formation [7]. The most common method in preparing frits today is sintering a portion of packed beads [8,9]. Silica particles are connected to each other at their contact points in a hydrothermal process. Frits prepared this way also possess good permeability and a constant electroosmotic flow (EOF). A disadvantage exists that the surface of beads in the frit is reactivated in the sintering process. An improved method is to re-deactivate the frits by recoating the frit surface with silane. It was found that the adsorption on the re-deactivated frits could be significantly reduced [10]. Furthermore, it was shown that recoating the frits also reduces the bubble formation in the columns [11]. In recent years there is a renaissance of using the sol–gel method [12–15] and taking advantage of photopolymers in

* Corresponding author. Tel.: +1 319 335 3167; fax: +1 319 335 1270.
E-mail address: lei-geng@uiowa.edu (L. Geng).

0021-9673/$ – see front matter © 2004 Published by Elsevier B.V.
doi:10.1016/j.chroma.2004.11.052

frits preparation [16]. These new methods avoid destructive heating on both beads and column and also have been claimed to produce frits with reduced bubble formation. In a recent report, the performances of frits prepared with sol–gel, sintering, photopolymerization and modified sol–gel technologies are evaluated [17]. It is shown that the modified sol–gel and photopolymerized frits show improved day-to-day and column-to-column reproducibilities. However, the sintered frits are still associated with the least amount of peak dispersion [17]. The new methods are still in their developing stages while sintering a portion of packing material may still be the most widely adopted frit preparation method in packed-column capillary electrochromatography.

In preparing routinely used columns and inventing new methods for frit preparation, permeability, reproducibility and dispersion caused by the frits are important parameters that researchers are most interest in. The overall performance of a frit is usually characterized using traditional EOF method [10,11,16,17]. Furthermore, it is more recognized recently that bubble formation in the CEC capillary is highly related to the frits [1,2,7,12,18]. It is desirable to directly visualize the underlying properties, e.g., the packing quality, deformation of sintered beads, and the surface-adsorption of a frit, to correlate with separation parameters obtained in the traditional EOF method.

Microscopic imaging has received much attention to study the fundamentals of separation since it approaches microscopic phenomena directly [19–24]. Scanning electron microscopy (SEM) has been extensively used to study the packing of both the frits and column [6,9,12,15,16]. A column containing the frit is usually cut into halves in the middle and the cross-section is imaged. The spatial resolution of electron micrograph is high, allowing fine details of CEC packings to be examined. However, due to the restriction of the experimental conditions of SEM, the observation could only be made in dry environment and static conditions. Phenomena and properties related to the frits under real chromatographic conditions, e.g., analyte-stationary phase interaction, and air bubble formation, cannot be observed using SEM. Guiochon and co-workers used direct photographic imaging to study the separation phenomena in situ [21–24]. Considerable amount of new information on packing bed heterogeneity, sample injection, migration, diffusion, and separation-related phenomena in liquid chromatography was obtained by photographic imaging.

Another approach is reported by Lowry et al. to study the solute distribution in CEC using laser scanning confocal fluorescence microscopy [19]. It has been shown that confocal fluorescence microscopy provides not only high contrast between chromatographic beads and their surrounding environment, but also excellent spatial resolution to image thin slices of the interior of chromatographic beads in situ for the first time. More importantly, the confocal imaging system provides good temporal resolution to observe the dynamic processes under real chromatographic conditions. In this paper, we extend this technique to study the frits structure and frits-associated bubble formation in capillary electrochromatography.

2. Experimental

2.1. Chemicals

Rhodamine6G was purchased from Aldrich (Milwaukee, WI). HPLC grade acetonitrile was obtained from Fisher (Fair Lawn, NJ). Luna silica beads used in frit preparation and CEC packing were obtained from Phenomenex (Torrance, CA). The 10 μm beads are C18 modified, and have a surface coverage of 17.5%, an average particle size of 10 μm, and average pore size of 100 Å. The coverage of bonded phase is 3.00 μmol/m^2. The 7 μm particles are uncoated, and have an average pore size of 100 Å. Deionized water was purified with a MilliQ system (MilliQ-Plus, Millipore, Bedford, MA) and was used to prepare all aqueous solutions. Refractive index matching oil (n = 1.51) was obtained from Carl Zeiss Microimaging Inc. (Thornwood, NY). Polyimide-coated capillaries (50 μm i.d., 360 μm o.d.) and non-coated quartz tubing (400 μm i.d., 550 μm o.d.) were acquired from Polymicro Technologies (Phoenix, AZ).

2.2. Capillary electrochromatograhy

Frits are prepared with four different methods: (1) sintering packed bare silica beads wetted with silicate solution; (2) sintering packed bare silica beads wetted with water; (3) sintering packed C18 silica beads wetted with water; (4) frits made using method (3) and then the surface of the beads is recoated with C18.

For the first method, a procedure was developed similar to established procedures in the literature [5] and described elsewhere [19,25,26]. Briefly, a segment of 50 μm i.d. capillary tubing was conditioned with 0.1 M NaOH for 20 min. The preconditioned capillary was then cut into 10 cm pieces. The polyimide coating was burned off with a small flame of a microtorch. Five milligram 7 μm uncoated silica beads and 3 μL Na_2SiO_3:H_2O (v/v) = 1:1 solution are mixed and stirred to form a paste. One end of the capillary was pressed into the paste to take up a few millimeters of the mixed materials. A thermal wire stripper was used to heat the sodium silicate mixture to form a frit at the end of the capillary.

The frits made from methods 2–4 are prepared with modified procedures in the literature [6]. Briefly, a preconditioned 50 μm i.d. capillary was stripped off coating and then cut into 10 cm pieces. One end of the capillary was fritted using method 1 as mentioned above as a temporary frit. The capillary was then packed with chromatographic beads using a vacuum pump. In method 2, 7 μm uncoated beads are packed while in methods 3 and 4 the 10 μm C18 beads are packed. The packing was then wetted and compressed using a syringe pump by pumping acetonitrile toward the temporary frit. Acetonitrile was then rinsed off with water

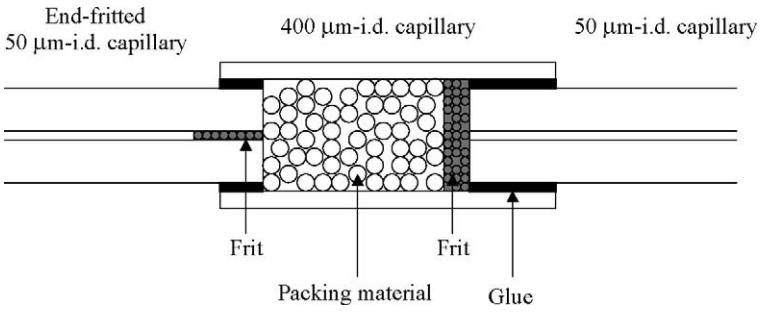

Scheme 1.

also using a syringe pump. A small section of the packing was sintered to form the desired frit. The temporary frit was cut and the rest of the packing material was flushed away. For method 4, the C18 recoating followed procedure of Carney et al. [11]. The fritted end was dipped into a 5% chlorodimethyloctadecylsilane (ODS) (Phase Separation Ltd., Deeside) solution for 5 s and dried in oven at 60 °C for an hour. The frits were soaked with 1 μM rhodamine6G solution by pumping 1 mL corresponding solutions through the capillary. The images were acquired with the solution inside the column.

For the observation of air bubble formation, a larger i.d. column was used, which favors the bubble formation (Scheme 1). A segment of 400 μm i.d. quartz tubing was conditioned with 0.1 M NaOH for 20 min. The tubing was cut into segments of 5 cm in length. One end of the tubing was pressed into the same paste of sodium silicate and 7 μm beads repeatedly to take up around 2 mm of the paste. The segment of paste was pushed into the tubing for ∼5 mm with a 50 μm i.d. capillary, and then sintered. An open capillary with 50 μm i.d. and 50 cm in length was glued to this end. The frit could serve as either the inlet or the outlet frit. C18 modified silica beads were then packed into the quartz cell against the frit by a vacuum pump to ∼2 cm in length. The second frit is prepared at the end of a 50 cm long, 50 μm i.d. capillary using method 1 mentioned above. The end-fritted 50 μm i.d. capillary was glued to the open end of the quartz cell to seal the packing materials. The column made from this method always has 1–2 mm unpacked region between the two frits after electrokinetic compaction.

A power supply manufactured by Spelman (model CZE1000PN30, Hauppauge, NY) provided the high voltage in CEC. The current was continuously monitored with a picoammeter (model 486, Keithley Instruments Inc., Cleveland, OH). A syringe pump was used to rinse the column with mobile-phase solution between experiments. The capillary was conditioned with the mobile phase for at least 50 column volumes before the solute solution was injected. In the CEC runs, several mobile phase compositions were used: a mobile phase containing 80% acetonitrile and 20% borate buffer at a concentration of 4 mM and pH 7.0, and a second mobile phase containing 50% acetonitrile and 50% phosphate buffer at a concentration of 4 mM and pH 7.0. In the bubble formation experiments, the buffer concentration was purposely raised to 50 mM with 80% acetonitrile and 20% buffer at pH 7.0.

2.3. Confocal imaging

The confocal imaging system has been described previously [19]. An inverted confocal microscope (Axiovert 100, LSM 510 scan module, Carl Zeiss Inc., Thornwood, NY) was used. The capillary was glued onto a standard glass microscope slide and capped with a coverslip. Two short pieces of capillary with the same o.d. serve as spacers to support the coverslip and confine the refractive index-matching fluid. Refractive index matching is essential to obtaining an undistorted image with a narrow depth of field. This is accomplished by reducing refraction from the capillary walls. The fluid also promotes heat transfer during electrophoresis. The capillary, fixed between the two slides, was placed on the microscope stage with the frits or packed zones directly over the objective.

A helium–neon laser (Uniphase, 1674P) provided excitation at 543 nm with laser power regulated by acoustooptical tunable filters. A 40× (NA 1.3) oil immersion objective was used to focus the laser beam into the sample and to collect the fluorescence emission. The spectral range of fluorescence emission was selected using the appropriate bandpass or long-pass filter. Fluorescence was directed through an adjustable pinhole and detected by a photomultiplier tube. The intensity is digitized with a 12-bit digitizer to yield pixel counts up to 4095. Each image acquired from the LSM instrument is stored as a data matrix. The digital image is directly displayed without any further treatment or modification.

3. Results and discussion

3.1. Frit structure

Four different types of frits were prepared from sintering beads and studied with confocal fluorescence imaging: (1) 7 μm unmodified silica beads wetted with sodium silicate; (2) 7 μm unmodified silica beads wetted with water; (3) 10 μm C18 silica beads wetted with water; and (4) 10 μm C18 beads wetted with water and then recovered C18 on the frit surface.

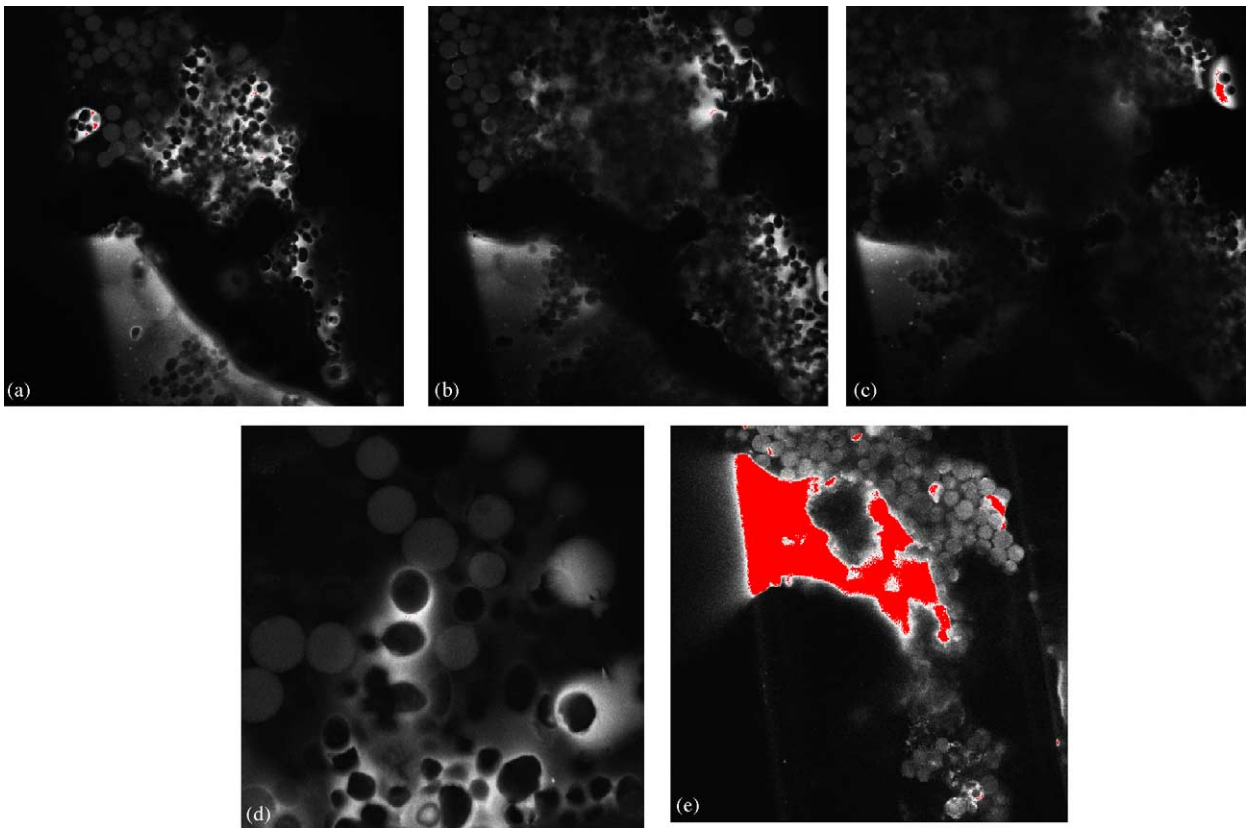

Fig. 1. Confocal fluorescence images of frits prepared from 7 μm unmodified porous silica beads wetted with sodium silicate. The frits were made in a 400 μm i.d. quartz tubing and then packed with 10 μm reversed phase chromatographic beads. The mobile phase is 80% acetonitrile and 20% 4 mM borate buffer at pH 7.0 with 1 μM rhodamine6G: (a–c) cross-sectional images of the same frit at $z = 18.55$, 30.20, 40.98 μm from the inner-wall of the capillary; (d) a magnified portion of the same frit; (e) a different frit showing strong solute adsorption in the polysilicate network; $z = 30.75$ μm from the inner wall of the capillary. Image size: 230 μm × 230 μm in 512 × 512 pixels. Acquisition time at each pixel: 2.56 μs.

Fig. 1a–c shows the images of the same type 1 frit made from sintering 7 μm porous silica beads wetted with sodium silicate in 400 μm i.d. fused silica column. In the imaging, the capillary is placed in the plane perpendicular to the optical axis of the microscope objective. The images are cross-sections at different depths of focus into the column. The column is packed with 10 μm C18-modified porous silica beads and filled with 1.0 μM rhodamine6G. A portion of the packing zone and the frit are in the image simultaneously. Judging from the sizes, the bigger bright circles in the image are the packing materials and the smaller dark circles are the beads sintered in the frit. The mobile phase has very low fluorescence and is shown as the background in the packed column. The intensity level of each pixel reflects the fluorophore concentration at that spatial location, since the fluorescence quantum yield of rhodamine6G does not vary significantly between different environments. The local concentration is determined by the partition coefficient between the mobile phase and the local environment at the specific pixel. Thus the contrast in the images is determined by the partition of the fluorescent molecules. Furthermore, quantitative information such as the concentration ratios and thus the partition coefficients can be obtained through the pixel intensities with appropriate calibration. In this paper, however, the images are analyzed qualitatively to describe the frit structure.

The frit made from sintering sodium silicate-wetted beads is not homogeneous. Upon close examination of the images, three types of image regions are identified (Fig. 1a–c): (A) dark beads embedded in bright media; (B) extended bright areas; and (C) extended dark areas. The bight media is assigned to the polysilicate network where fluorescent molecules have been adsorbed. The structure of type A image regions is ideal for a CEC frit: the silica beads serve as the framework while the polysilicate network glue them together and attach the frit to the wall of the capillary. The extended bright area is assigned to polysilicate network without beads. This type of structure seems inevitable because: (1) the mixing of 7 μm beads and silicate solution is incomplete and (2) the beads will not fill all the space in the column—the paste is so viscous that it cannot flow freely to form a plug with smooth surfaces in the column, with the empty space filled by the solution. The extended dark areas are gaps between fragments of the sintered frits. They are introduced in the repeatedly tapping procedure when filling the column with the paste. Since the fluorescent dye has high affinities to the polysilicate network and the stationary phase, concentration of fluorescent molecules is very low in these gaps filled with the mobile

phase, resulting in dark areas of the image. These areas tend to appear close to the inner wall of the column, e.g., 18 μm from the wall in Fig. 1a. When the focusing plane was moved further into the column to a depth of 41 μm, the gap area is reduced significantly. However, the imaging quality is reduced at this depth due to the increased scattering along the laser path.

The silicate network is continuous and highly fluorescent, which indicates that it is accessible to the solvent and it adsorbs fluorescent solute molecules. Meanwhile, the 7 μm porous silica beads packed in the frit are dark, indicating that the interior of the beads is not accessible to the solvent, thus non-accessible to the fluorescent dye. The porous structure on the surface of the beads was possibly destroyed in the sintering process in the presence of silicate that the nanopores of the beads were blocked. Since the interior of 7 μm beads is not accessible to the mobile phase, the EOF generated at the frit should basically come from the polysilicate network. The imaging study shows that the polysilicate network not only serves as 'glue' to hold beads together but also is the major contributor to the EOF generated at the frit.

The polysilicate network does not show equal fluorescence intensity everywhere, indicative of heterogeneous surface properties. In a few instances, extraordinarily strong solute adsorption occurs in the polysilicate network. The fluorescence from these adsorption sites is so intense that it is impossible to image the adsorption spot and the surroundings simultaneously due to the high contrast (Fig. 1e). The adsorption of solute molecules on the frit surface is not favorable in making a column, because it causes tailing and decreases the sensitivity of the capillary. We noticed that the surface properties of the polysilicate are hard to control and reproduce in the sintering process.

Frits made from sintering beads–silicate paste assume irregular geometric shapes at the boundary. This is because the paste packed into the column takes random shapes due to its viscous nature. There are corners and gaps left unfilled on the edge of the frit. C18 beads are easily packed into these unfilled spaces in column preparation. In a contact region between the packing material and the frit, both C18 beads and bare silica beads are imaged (Fig. 1d). The irregular boundary of the frit will cause inhomogeneity of the EOF across the column. As discussed above, the distribution of 7 μm beads in the frit is not homogeneous either, which will worsen the EOF generated at the frit. The gaps in the frit could potentially cause problems such as inhomogeneity of permeability of the frit. The extent of the structural irregularities, such as the uneven boundary of the frit, the inhomogeneous packing of the 7 μm beads, gaps in the frit, vary for each individual frit. Practically, these irregularities are difficult to avoid. The bigger the column, the more challenging to make the frits uniform. Compounded with difficulties in controlling surface properties of polysilicate network in the sintering process, all these are practical problems to overcome for this preparation method.

We then studied the frits prepared from more recent procedures. Fig. 2a shows the frit made from 7 μm bare silica beads wetted with water. Fig. 2b depicts a frit sintered from 10 μm C18 porous beads in 50 μm column. Fig. 2c shows a frit prepared from method 3 after which the surface C18 was recovered. The C18 recovery on the surface of the beads is quite uniform judging from the fluorescence intensity of the beads. For all three methods, the packing of beads in the frits is similarly homogeneous. This is because in the absence of viscous sodium silicate, the beads move more freely and are packed tightly under external pressure. The inside of the beads is bright except for a few nonporous C18 beads [19]. This is an indication that the porous structure of the beads is not altered during the sintering process and the pores are still accessible to the mobile phase. Thus, the EOF generated at the frit is mainly determined by the surface properties of the beads. The beads remain circular in shape in most part. In contact points the beads are slightly deformed and glued together. The fluorescence intensity is uniform and no obvi-

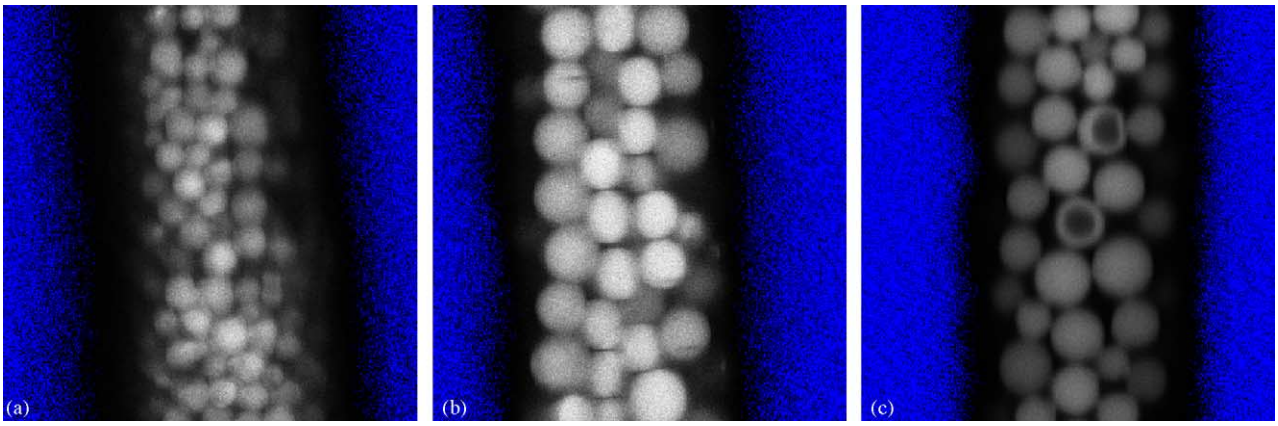

Fig. 2. Frits made from sintering (a) 7 μm bare silica beads wetted with water in 50 μm i.d. column; (b) C18 beads wetted with water in 50 μm i.d. column; (c) C18 beads wetted with water in 50 μm i.d. column and then recovered with C18. The column was soaked in solution of 80% acetonitrile and 20% 4 mM borate buffer at pH 7.0 with 1 μM rhodamine6G. Image size: 76.8 μm × 76.8 μm in 512 × 512 pixels. Acquisition time at each pixel was 3.2 μs for (a) and 1.6 μs for (b) and (c).

ous strong fluorescent sites are observed as in the type 1 frits. Judging from the packing homogeneity of the frits, sintering chromatography beads wetted with water provides good frits for CEC separation.

In the above studies, confocal fluorescence microscopy not only provides high contrast between chromatographic beads and the surrounding environment, but also makes it possible to image thin slices of the interior of a column with high spatial resolution, and to construct three-dimensional images of the packed column. It is the fluorescence that allows us to assess whether the interior of a chromatographic bead is accessible to the solvent. Such information is not available from transmission microscopy.

3.2. Bubble formation

Air bubble formation is one of the biggest practical problems in CEC. Why and how the bubbles form are still not clear [1,2]. The early theory was that bubbles form due to joule heating as evidenced by the higher propensity of bubble formation with wider capillaries and higher electrolyte concentrations [27]. More recently, there are indications that self-heating is not the primary cause, e.g., the electric current in CEC is one to two orders of magnitude lower than those of capillary electrophoresis (CE) or micelle electrokinetic chromatography (MEKC). Pyell observed that bubbles form invariably at the border between the packed and the unpacked sections of the capillary in semi-packed column [7]. Works by Pyell and others suggest that the different rates of EOF at different segments cause the intersegmental pressure that leads to bubble formation [7,28,29]. It has also been shown that the low mechanical streaming permeability is an important factor that leads to the bubble formation [11].

We demonstrate in this paper that confocal fluorescence microscopy has both the spatial and the temporal resolution to observe the bubble formation in situ. Generation of air bubbles was observed in a 400 μm i.d. packed column as described in the experimental section. The packing material is 10 μm C18 beads and the total length of the packing is around 1.5 cm. The packing was sealed between a frit in the same column at one end (400 μm i.d. end) and an end-fritted column with 360 μm o.d. glued at the other end (50 μm i.d. end) (Scheme 1). Since the end-fritted column was glued on, the packing is not very tight and the space between the two frits is not completely filled. Columns made with this method always have a short segment (around 1 mm) unfilled between the two frits after the packing material has been wetted and repacked with an applied solvent flow under EOF or flow generated by a syringe pump. When a high voltage is applied on the column, the chromatographic beads are negatively charged and the electrophoresis will force them to move toward the anode while the electroosmotic flow pushes them toward the cathode. The net flow direction of the beads is the same as the EOF under our experimental conditions. Thus the chromatographic beads will be packed against the outlet frit. The short segment of unfilled column will cause packing bed reorganization if we reverse the flow direction. We noticed that this packing bed reorganization is a primary cause of air bubble formation at the outlet frit in a CEC run.

Fig. 3 shows the bubble formation at the outlet frit during such a packing bed reorganization process. Before the chromatographic run, the column was flushed with running buffer against the frit at 50 μm i.d. end to exclude any bubbles. The entire column, including the packing zone, the frits, and the region of open capillary, is examined under microscope to make sure it is devoid of air bubbles. The high voltage is then applied such that the EOF moves the solution toward the 50 μm i.d. end. There is no packing bed reorganization when HV applied since there is no change in flow direction. The column is stable under this condition for more than an hour. The electric current is stable around 1.70 μA and there are no air bubbles generated during the run under microscope examination. The first image of Fig. 3 shows the portion close to the inlet frit. The lower part of the images is the frit. There is also some packing material fused with the frit. Above the frit, it is the unfilled packing zone. However, the packing is not seen in the image because they are packed against the other end of the column.

After the high voltage was reversed, in first a few images the packing materials are moving toward the outlet frit. In image 2 taken at 19.60 s, a first visible air bubble is formed and appears in the image as a dark circle. The bubble is then pushed against the capillary wall by the incoming packing beads. This bubble keeps growing larger in the ensuing images. The packing materials are observed to be moving into the imaging area and undergoing reorganization. In the image taken at 58.80 s, another air bubble (lower bubble) appears at a place closer to the frit. Both bubbles are growing afterwards. It is interesting to note that the position of the lower bubble is changing from time to time. In the images taken at 82.32 and 94.08 s, it disappeared from the observation area. Since it came back in later images at the same location, we assume that this bubble was squeezed out of the imaging plane temporarily by the moving packing beads. In the image taken at 109.76 s, the lower bubble grew very big and the wall that separates the two air bubbles is very thin. In the next image, the lower air bubble disappeared permanently from the image, later proved by examining the optical sections at different z planes of the column under the microscope. Our interpretation is that it merged with the upper bubble to form a huge air pocket and eventually blocked the column. The electric current dropped to 7.0 nA at the end of the chromatographic run.

In Fig. 4, we imaged this huge air bubble in the column at different z planes. This bubble starts from the wall of the capillary at one end and adopts an interesting seashell shape. The bubble takes up the majority of the space across the column within the practical imaging depth, which is ∼50 μm. The electric current dropped to only 0.4% of the initial value. It practically clogs the column.

The whole process of the bubble formation took around 150 s. The time resolution between images in the recording

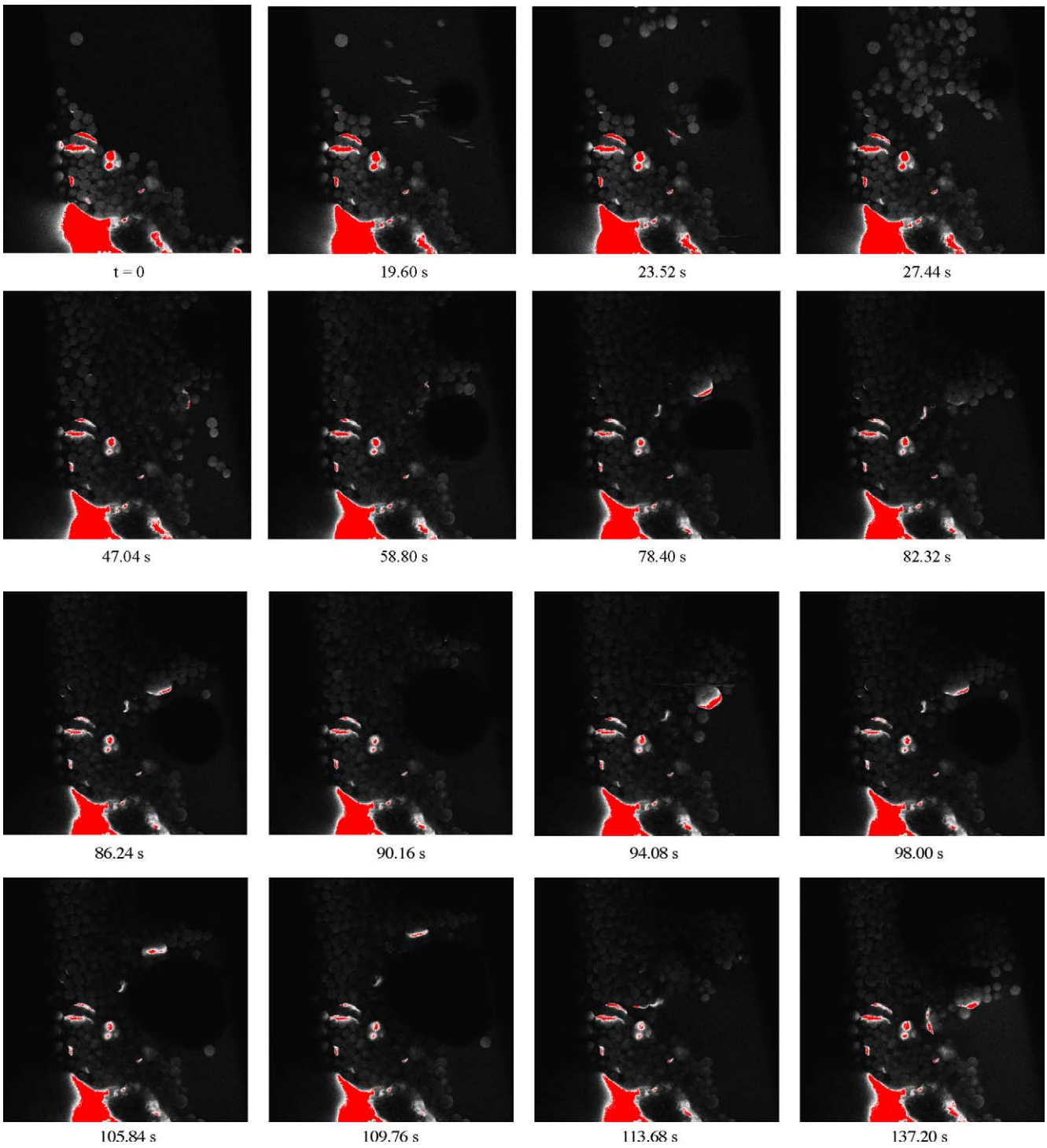

Fig. 3. Selected images of bubble formation close to the frit inside a 400 μm i.d. column packed with 10 μm C18 beads. The mobile phase solution was 80% acetonitrile and 20% of 50 mM borate buffer at pH 7.0 with 1 μM rhodamine6G. High voltage applied: 25 kV. Image size: 230 μm × 230 μm in 512 × 512 pixels. Acquisition time at each pixel: 1.6 μs. Images are labeled with times when they were collected.

was 3.92 s. Bubbles forming and merging are successfully observed at the border between the packing material and the frit. It is also possible that bubbles observed in consecutive frames are not the same one but two bubbles formed repetitively at the same location with the former one flushed out of the image with a sudden translocation. With current time resolution, these two possibilities are not differentiated. The presented images are acquired with 1 μM rhodamine6G. To improve the time resolution, higher concentration of fluorophores, and/or detection systems with higher sensitivities could be used to reduce the integration time. The size of the images could be reduced to a quarter of the original

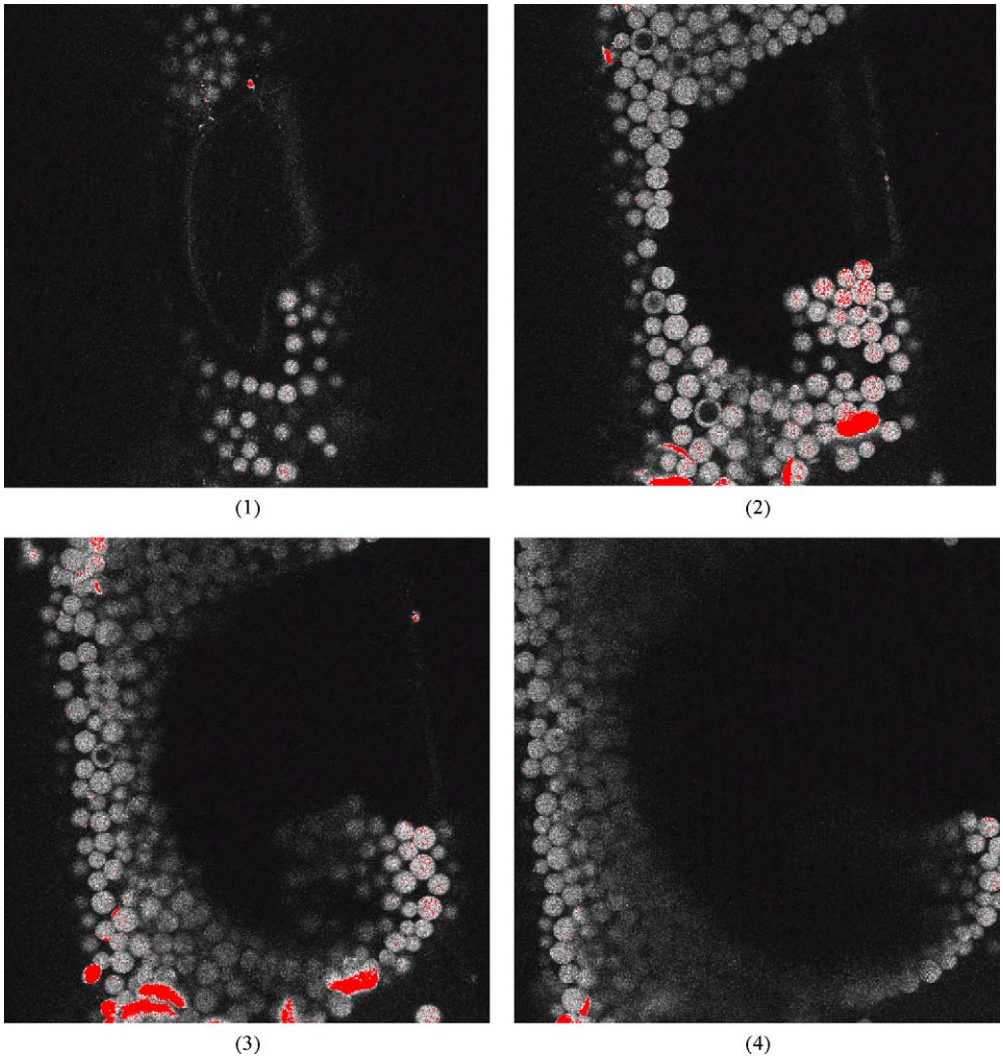

Fig. 4. The z-sections of a bubble generated at the boundary between the packing material and the frit; $z = 0.96, 10.57, 20.18, 35.55$ μm from the inner wall of the capillary. Image size: 230 μm × 230 μm in 512 × 512 pixels. Acquisition time at each pixel: 1.6 μs. Other conditions are the same as in Fig. 3.

size (512 × 512) if higher time resolution is needed. In general, the acquisition time of each image could be reduced to below one second. With such a time resolution, many dynamic phenomena in the capillary could be directly observed, such as air bubble reorganization and packing bed movement [30].

How and why the air bubble is generated is still elusive. However, several conclusions could be drawn from our imaging experiments. First, the air bubbles are generated in the packed section of the column. Second, the air bubble tends to grow at or close to the border of the frit. At present, it is unclear whether the air phase is generated at the border between the packing material and the frit, or generated in the column and brought to the frit. Repeated observations support that visible bubbles finally reside at the outlet frit. Thus the permeability plays a potential role in the development of air bubbles. Third, the reorganization of the packing bed seems to increase the probability of bubble formation. Generally, if bubbles do not form during the bed reorganization process, the probability is low that bubbles will form at a later time in the same run. Fourth, just from the imaging experiments, it is difficult to determine which factor is more important, EOF difference between the frit and the packing, or the joule heating. The bubbles do occur at the border of the packing material and the frit, which seems to support the EOF theory. On the other hand, we purposely increased the ionic strength and used larger capillaries to raise the probability of observing air bubble formations. This means joule heating could also play an important role. It is possible that both factors are important in bubble formation.

The column we made is asymmetric and we can use either end as the inlet end. In our experiment, we observed that air bubbles generate at either end and always at the outlet end. The reason that we made the observation at the 400 μm i.d. end is for imaging purpose so that we can observe both the packing and the frit simultaneously.

4. Conclusions

Confocal fluorescence microscopy provides a convenient and nondestructive way to study the three-dimensional structure of the packing and frits in CEC. Frits prepared with sintering beads soaked with silicate have the highest heterogeneity in the four types of frits studied. There are regions of beads connected by polysilicate network, purely silicate network, and gaps between frit fragments. The pores of the sintered beads could be blocked in the sintering process thus the EOF generated from this type of frit may be primarily determined by the polysilicate network. The surface property of the polysilicate network is difficult to control and in some cases strong adsorption occurs. The other three types of frits have similar homogeneity of packing and no strong adsorption was observed.

Packing bed reorganization induces air bubble formation in CEC separation. Permeability plays an important role in the growth of air bubbles. Although the spatial resolution of confocal fluorescence microscopy is not as high as SEM, it provides the capability of observing dynamic processes in real time, under real chromatographic conditions. Confocal fluorescence spectroscopy opens a new avenue to study dynamic processes in situ in chemical separations.

Acknowledgments

This work is supported by a Biosciences Initiative Grant from the University of Iowa. G.W. thanks the Center of Biocatalysis and Bioprocessing of the University of Iowa for a predoctoral fellowship.

References

[1] U. Pyell, J. Chromatogr. A 892 (2000) 257.
[2] L.A. Colón, G. Burgos, T.D. Maloney, J.M. Cintron, R.L. Rodriguez, Electrophoresis 21 (2000) 3965.
[3] H.J. Cortes, T.S. Pfeiffer, B.C. Richter, J. High Resolut. Chromatogr. (1987) 446.
[4] K.W. Whitaker, M.J. Sepaniak, Electrophoresis 14 (1994) 1341.
[5] R.T. Kennedy, J.W. Jorgenson, Anal. Chem. 61 (1989) 1128.
[6] B. Behnke, E. Grom, E. Bayer, J. Chromatogr. A 716 (1995) 207.
[7] H. Rebscher, U. Pyell, Chromatographia 42 (1996) 171.
[8] N.W. Smith, M.B. Evans, Chromatographia 38 (1994) 649.
[9] R.J. Boughtflower, T. Underwood, C.J. Paterson, Chromatographia 40 (1995) 329.
[10] B. Behnke, J. Johansson, S. Zhang, E. Bayer, S. Nilsson, J. Chromatogr. A 818 (1998) 257.
[11] R.A. Carney, M.M. Robson, K.D. Bartle, P. Myers, J. High Resolut. Chromatogr. 22 (1999) 29.
[12] Y. Chen, G. Gerhardt, R. Cassidy, Anal. Chem. 72 (2000) 610.
[13] M. Schimid, F. Bauml, A.P. Kohne, T. Welsch, J. High Resolut. Chromatogr. 22 (1999) 438.
[14] X. Zhang, S. Huang, J. Chromatogr. A 910 (2001) 13.
[15] M. Kato, M.T. Dulay, B.D. Bennett, J.P. Quirino, R.N. Zare, J. Chromatogr. A 924 (2001) 187.
[16] J. Chen, M.T. Dulay, R.N. Zare, F. Svec, E. Peters, Anal. Chem. 72 (2000) 1224.
[17] S.M. Piraino, J.G. Dorsey, Anal. Chem. 75 (2003) 4292.
[18] H. Rebscher, U. Pyell, Chromatographia 38 (1994) 737.
[19] M. Lowry, Y. He, L. Geng, Anal. Chem. 74 (2002) 1811.
[20] R.A. Shalliker, B.S. Broyles, G. Guiochon, J. Chromatogr. A 994 (2003) 1.
[21] U. Tallarek, E. Rapp, H. Sann, U. Reichl, A. Seidel-Morgenstern, Langmuir 19 (2003) 4527.
[22] R.A. Shalliker, B.S. Broyles, G. Guiochon, Anal. Chem. 72 (2000) 323.
[23] R.A. Shalliker, B.S. Broyles, G. Guiochon, J. Chromatogr. A 865 (1999) 83.
[24] T. Yun, G. Guiochon, J. Chromatogr. A 760 (1997) 17.
[25] Y. He, L. Geng, Anal. Chem. 73 (2001) 5564.
[26] Y. He, L. Geng, Anal. Chem. 74 (2002) 1819.
[27] J.H. Knox, I.H. Grant, Chromatographia 32 (1991) 317.
[28] A.S. Rathore, C. Horvath, Anal. Chem. 70 (1998) 3069.
[29] L.A. Colón, Electrophoresis 18 (1997) 2162.
[30] M. Lowry, G. Wang, Z. Zhong, L. Geng, manuscript in preparation.